J|A|C|S
ARTICLES
Published on Web 12/12/2003

Chemically Distinct Ni Sites in the A-Cluster in Subunit β of the Acetyl-CoA Decarbonylase/Synthase Complex from *Methanosarcina thermophila*: Ni L-Edge Absorption and X-ray Magnetic Circular Dichroism Analyses

Tobias Funk,[†] Weiwei Gu,[‡] Stephan Friedrich,[§] Hongxin Wang,[‡] Simonida Gencic,[||] David A. Grahame,*[,||] and Stephen P. Cramer*[,†,‡]

Contrbution from the Physical Biosciences Division, Lawrence Berkeley National Laboratory, Berkeley, California 94720, Department of Applied Science, University of California, Davis, California 95616, Advanced Detector Group, Lawrence Livermore National Laboratory, Livermore, California 94550, and Department of Biochemistry and Molecular Biology, Uniformed Services University of the Health Sciences, Bethesda, Maryland 20814

Received June 10, 2003; E-mail: dgrahame@usuhs.mil

Abstract: The 5-subunit-containing acetyl-CoA decarbonylase/synthase (ACDS) complex plays an important role in methanogenic Archaea that convert acetate to methane, by catalyzing the central reaction of acetate C−C bond cleavage in which acetyl-CoA serves as the acetyl donor substrate reacting at the ACDS β subunit active site. The properties of Ni in the active site A-cluster in the ACDS β subunit from *Methanosarcina thermophila* were investigated. A recombinant, C-terminally truncated form of the β subunit was employed, which mimics the native subunit previously isolated from the ACDS complex, and contains an A-cluster composed of an $[Fe_4S_4]$ center bridged to a binuclear Ni−Ni site. The electronic structures of these two Ni were studied using L-edge absorption and X-ray magnetic circular dichroism (XMCD) spectroscopy. The L-edge absorption data provided evidence for two distinct Ni species in the as-isolated enzyme, one with low-spin Ni(II) and the other with high-spin Ni(II). XMCD spectroscopy confirmed that the species producing the high-spin signal was paramagnetic. Upon treatment with Ti^{3+} citrate, an additional Ni species emerged, which was assigned to Ni(I). By contrast, CO treatment of the reduced enzyme converted nearly all of the Ni in the sample to low-spin Ni(II). The results implicate reaction of a high-spin tetrahedral Ni site with CO to form an enzyme-CO adduct transformed to a low-spin Ni(II) state. These findings are discussed in relation to the mechanism of C−C bond activation, in connection with the model of the β subunit A-cluster developed from companion Ni and Fe K edge, XANES, and EXAFS studies.

Introduction

A wide range of anaerobic Bacteria and Archaea employ a unique organometallic enzymatic mechanism involving several different metal-bound carbon species (acetyl, CO, and methyl) for direct synthesis and/or cleavage of the C−C bond of acetate. Metabolic pathways that use direct acetyl C−C bond activation include the energy-requiring autotrophic fixation of CO_2, as well as processes used for energy production such as acetogenesis from CO_2 and H_2, oxidation of acetate to 2 CO_2, and disproportionation of acetate to CO_2 and CH_4. Approximately two-thirds of the nearly 10^9 tons/year of CH_4 formed in the environment by microorganisms are derived from cleavage of acetate by methanogens. Cleavage of the acetyl C−C bond is brought about by an enzymatic decarbonylation reaction catalyzed by a multienzyme complex designated acetyl-CoA decarbonylase/synthase (ACDS).

The ACDS complex is composed of five different subunits (α, β, γ, δ, and ϵ),[1,2] and in addition to C−C bond cleavage, it also catalyzes several other partial reactions.[3] These include the oxidation of the carbonyl group of acetyl-CoA to CO_2 and the transfer of the methyl group to the acceptor substrate tetrahydrosarcinapterin (H_4SPt), an analogue of tetrahydrofolate, forming N^5-methyltetrahydrosarcinapterin (CH_3-H_4SPt), in the overall reaction, as follows.[2]

$$\text{Acetyl-CoA} + H_4\text{SPt} + H_2O \rightleftarrows \text{CoASH} + CH_3-H_4\text{SPt} + CO_2 + 2H^+ + 2e^- \quad (1)$$

The active site for C−C bond cleavage is located in the ACDS β subunit which harbors a unique heterometallic center known as the A-cluster, which contains an $[Fe_4S_4]$ unit and 2 Ni. Site-directed mutagenesis studies have shown that an intact A-cluster is required for acetyl transfer activity, forming an acetyl-enzyme

[†] Physical Biosciences Division, Lawrence Berkeley National Laboratory.
[‡] Department of Applied Science, University of California, Davis.
[§] Advanced Detector Group, Lawrence Livermore National Laboratory.
[||] Department of Biochemistry and Molecular Biology, Uniformed Services University of the Health Sciences.

(1) Terlesky, K. C.; Nelson, M. J. K.; Ferry, J. G. *J. Bacteriol.* **1986**, *168*, 1052−1058.
(2) Grahame, D. A. *J. Biol. Chem.* **1991**, *266*, 22 227−22 233.
(3) Grahame, D. A.; DeMoll, E. *J. Biol. Chem.* **1996**, *271*, 8352−8358.

10.1021/ja0366033 CCC: $27.50

species activated for C−C bond cleavage, reaction 2.[4]

$$E_\beta + \text{acetyl-CoA} \rightleftarrows E_\beta\text{-acetyl} + \text{CoA} \qquad (2)$$

Acetyl transfer is strictly dependent on low redox potential, with half-maximal activity observed at −486 mV at pH 6.5. Reductive activation of the enzyme takes place according to a 1-electron redox process, which suggests that Ni(II) present in the as-isolated enzyme is reduced to Ni(I), which then would carry out nucleophilic attack on acetyl-CoA.[5] A corrinoid cofactor located on the ACDS $\gamma\delta$ protein subcomponent accepts the nascent methyl group formed upon cleavage of the C−C bond and transfers it to H_4SPt, whereas the ACDS $\alpha_2\epsilon_2$ subcomponent carbon monoxide dehydrogenase (CODH) oxidizes enzyme-bound CO derived from the carbonyl group.[3]

Two separate crystallographic structures have been reported for the A-cluster in carbon monoxide dehydrogenase/acetyl-CoA synthase (CODH/ACS), an $\alpha_2\beta_2$ homodimeric bacterial enzyme containing the A-cluster in the α subunit, which is homologous to the β subunit in ACDS from methanogens. The first structure revealed an A-cluster consisting of an $[Fe_4S_4]$ cluster bridged to a Cu−Ni binuclear site in which Cu was located proximal to the $[Fe_4S_4]$ cluster, designated M_a, whereas the distal site, M_b, was occupied by Ni in square planar geometry.[6] The second structure portrayed rather different metals in the proximal position, and contained two different A-cluster structures in separate α subunits displaying dissimilar conformational states.[7] One conformational state designated "open" contained an $[Fe_4S_4]$−Ni−Ni arrangement with the proximal Ni in square planar geometry, whereas the alternate "closed" state contained an $[Fe_4S_4]$−Zn−Ni form of the A-cluster, with Zn in tetrahedral geometry, analogous to the $[Fe_4S_4]$−Cu−Ni type in the first crystallographic study. In all cases, the distal Ni site was present in square planar geometry, coordinated by two cysteine thiolate groups and two deprotonated amides belonging to the protein backbone.

By contrast, the methanogen ACDS β subunit does not contain Cu or Zn, and evidence indicates an $[Fe_4S_4]$−Ni−Ni form of the A-cluster. K-edge X-ray absorption spectroscopic analyses of the β subunit A-cluster indicated that Ni was present in two different coordination environments, one approximately tetrahedral and the other square planar, together contributing to make up the overall XANES and EXAFS spectra observed.[8] On the basis of these results, a structure for the β subunit A-cluster was proposed similar to that in CODH/ACS, but with the proximal site of the binuclear center occupied by Ni in approximately tetrahedral geometry.[8]

Both native enzymes CODH/ACS and ACDS react with CO to generate an $S = 1/2$ paramagnetic enzyme-CO adduct detectable by EPR spectroscopy at temperatures up to ∼130 K, which is a property characteristic of the A-center (with EPR signal known as the NiFe−CO signal because of hyperfine broadening by ^{61}Ni or ^{57}Fe, or with ^{13}CO used in the reaction).[9−11] Using a recombinant form of the ACDS β subunit, Ni was shown to be essential both for activity and for the formation of the NiFe−CO EPR signal. Studies on CODH/ACS concluded that reduction of the enzyme was required prior to CO binding to generate the paramagnetic NiFe−CO species, formulated as Ni^{1+}−CO (or A_{red}−CO).[12] However, with the recombinant ACDS β subunit, reactions of the Ni(II)-containing enzyme with CO produce a strong EPR signal with equivalent intensity regardless of the presence or absence of reducing agent 1 mM Ti^{3+} citrate. This result provided evidence that Ni(I) was not involved in the paramagnetic A center-CO adduct, and a Ni-(II)−CO radical species was proposed.[4]

To better understand the electronic structure of the different Ni species in the A-cluster, we studied this system by Ni L-edge absorption and X-ray magnetic circular dichroism (XMCD) spectroscopies. The recombinant β subunit was examined under several different reaction conditions: as-isolated, in the presence of Ti^{3+} citrate, and with both Ti^{3+} citrate and CO. By comparison with model compound spectra, we estimate the fraction of different Ni oxidation and spin states under varying reaction conditions. The implications for distinct chemical properties of the proximal and distal Ni sites are discussed.

Experimental Procedures

General Procedures. Unless otherwise specified, all chemicals were purchased from Sigma Chemical Co. at the highest purity offered. All solutions were prepared using deionized water obtained by use of a Milli-Q apparatus (Millipore Corp.). Stock solutions of 140 mM Ti^{3+} citrate were prepared immediately before use as described,[5] and diluted with 25 mM HEPES, pH 7.2 to give working solutions containing 11−44 mM Ti^{3+}. Unless otherwise indicated, anaerobic procedures were carried out under an atmosphere of N_2 containing 1−3% H_2 using a Coy type anaerobic chamber. A calibrated Teledyne model 3191 trace oxygen analyzer was used to monitor O_2 levels, which were typically in the range of 0.5−2 ppm.

Protein Purification and Ni Reconstitution. Recombinant ACDS subunit β was obtained by anaerobic expression in *E. coli* of a 44.6 kDa, C-terminally truncated form of the *Methanosarcina thermophila* strain TM-1 ACDS β subunit with 85% of the molecular mass of the full length protein, designated CdhC*, as previously described.[4] This form mimics the truncated β subunit isolated following proteolytic dissociation of the native ACDS complex.[3] The recombinant protein which contained Fe but lacked Ni was purified by ion exchange chromatography under anaerobic conditions and reconstituted with Ni^{2+} by using the 'large scale' method exactly as previously described.[4] Following the step at which excess Ni^{2+} was removed by chromatography on Sephadex G-25, the holoenzyme was subjected to diafiltration on an Amicon YM 30 ultrafiltration membrane to concentrate the enzyme and reduce buffer and salt concentrations. The protein preparations were 90−93% pure as found by densitometric analysis of SDS gels, and contained 3.0 ± 0.2 g atom Fe/mol protein, as determined by ICP analyses and protein estimation methods described previously.[8] Samples of the Ni reconstituted protein exhibited an Fe/Ni ratio of 1.8 by ICP analysis.

Sample Preparation for Soft X-ray Spectroscopy. Samples for L-edge and XMCD measurements were prepared by applying 10 μL of the protein (0.28 mM CdhC* in low buffer and salt concentration, 3.2 mM HEPES, 0.8 mM Na_2SO_4, pH 7.2) to 6 mm diameter sapphire disks, followed by drying. Samples designated "as-isolated" were dried

(4) Gencic, S.; Grahame, D. A. *J. Biol. Chem.* **2003**, *278*, 6101−6110.
(5) Bhaskar, B.; DeMoll, E.; Grahame, D. A. *Biochemistry* **1998**, *37*, 14491−14499.
(6) Doukov, T. I.; Iverson, T. M.; Seravalli, J.; Ragsdale, S. W.; Drennan, C. L. *Science*, **2002**, *298*, 567−572.
(7) Darnault, C.; Volbeda, A.; Kim, E. J.; Legrand, P.; Vernéede, X.; Lindahl, P. A.; Fontecilla-Camps, J. C. *Nat. Struct. Biol.* **2003**, *4*, 271−279.
(8) Gu, W.; Gencic, S.; Cramer, S. P.; Grahame, D. A. *J. Am. Chem. Soc.* **2003**, *125*, 15343−15351.
(9) Ragsdale, S. W.; Ljungdahl, L. G.; DerVartanian, D. V. *Biochem. Biophys. Res. Commun.* **1983**, *115*, 658−665.
(10) Ragsdale, S. W.; Wood, H. G.; Antholine, W. E. *Proc. Natl. Acad. Sci.* **1985**, *82*, 6811−6814.
(11) Fan, C. L.; Gorst, C. M.; Ragsdale, S. W.; Hoffman, B. M. *Biochemistry* **1991**, *30*, 431−435.
(12) Russell, W. K.; Lindahl, P. A. *Biochemistry* **1998**, *37*, 10016−10026.

under an atmosphere of 1−3% H_2 in N_2 in a Coy anaerobic chamber operating at less than 2 ppm O_2, and required approximately 35 min to produce a thin dry film. Samples containing in addition 0.5−4 mM Ti^{3+} citrate were prepared by addition of 1/20 or 1/10 volume of Ti^{3+} working solutions (11−44 mM Ti^{3+}) and were similarly dried, and are designated as "Ti^{3+}-reduced". Samples designated "CO/Ti^{3+}-treated" were prepared identically except that drying was carried out under an atmosphere of 100% CO. This was accomplished by transferring the disks to a small chamber, ~3 cm^3 volume, through which 100% CO (Matheson, research purity grade, 99.99% minimum, <0.05 ppm O_2) was allowed to flow at a constant rate sufficient to dry the sample over a comparable time interval. Dried films exposed to the atmosphere of the anaerobic chamber for 21 h at room temperature and subsequently redissolved in anaerobic buffer exhibited high levels of acetyltransferase activity (assayed as described previously),[4] with 82−89% of the original activity remaining under nonreducing conditions and 61−64% in Ti^{3+}-reduced samples, with 100% activity equivalent to a turnover rate for acetyl transfer of 4500 min^{-1}. The disks were mounted in a capped sample holder under anaerobic conditions and transferred to a vacuum chamber as described previously.[13] The samples were kept inside the capped sample holder during transfer and the cap was removed only after the sample equilibrated with the coldfinger at temperatures below 50 K.

Soft X-ray Fluorescence Elemental Analysis. Standard solutions of $Fe(NH_4)_2(SO_4)_2$, and $NiCl_2$, in 0.01M HCl were mixed to produce samples containing 1.00 mM $NiCl_2$ and a range of $Fe(NH_4)_2(SO_4)_2$ from 1.00 to 8.0 mM, to provide solutions containing Fe:Ni ratios of 1, 2, 4, and 8. Thin film samples prepared from these standards, as well as an "as-isolated" ACDS β subunit sample, were excited at 890 eV, and the emission spectra were recorded with a custom designed 9-element superconducting tunnel junction (STJ) detector.[14] The Fe:Ni fluorescence ratio was obtained by integration and summation of all Fe and Ni L lines, after subtraction of the spectral baseline.

Soft X-ray Absorption and XMCD Spectroscopy. The experiments were conducted at the elliptically polarizing undulator beamline of the Advanced Light Source (ALS).[15] Tandem ultrahigh vacuum chambers permitted fluorescence-detected absorption measurements both with our custom-designed STJ detector[14] and with a Canberra 30-element Ge detector.[16] The STJ detector was attached to a chamber equipped with a helium flow cryostat operating at temperatures down to 16 K (L-edge chamber), whereas the Ge detector was mounted on a chamber equipped with a 6 T superconducting magnet (XMCD chamber) in which the sample stage was connected to a pumped He cryostat capable of reaching a base temperature of 2.2 K.[17] The chambers were maintained at a vacuum in the low 10^{-9} mbar region.

The ACDS β subunit data were recorded as fluorescence excitation spectra.[18] The Ni fluorescence signal (I_F) was obtained by integration of the Ni L$\alpha\beta$ regions of independent multichannel analyzer spectra for each detector element. To correct for incident beam intensity fluctuations, the Ni signal was divided by the incident beam intensity (I_0). A signal proportional to I_0 was measured using either the total electron yield from an Al foil placed between the sample and monochromator, or using the oxygen fluorescence signal from the sample itself. The exit slit was set to 20 μm, leading to an energy resolution of ~0.2 eV at 800 eV. The energy was calibrated using the total electron yield spectrum of NiF_2, with centroid energy of the L_3-line defined to be 852.7 eV.[19]

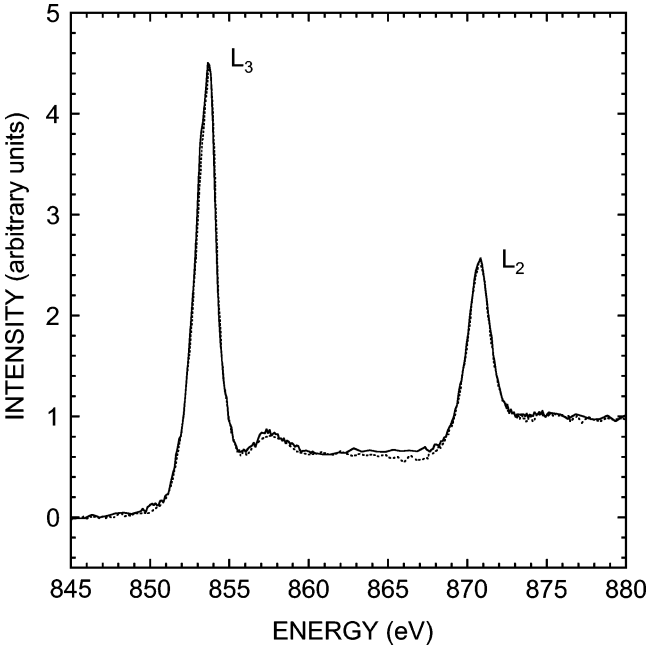

Figure 1. Ni L-edge spectra of the as-isolated ACDS β subunit taken with the STJ (- - -) and Ge (−) detectors. Separate enzyme samples were used, and conditions for measurements in the separate chambers were as described under Experimental Procedures.

Control Experiments for Radiation Damage. To ensure that the samples were not compromised due to exposure to the X-ray beam, different conditions were examined for the potential to cause radiation damage. When multiple spectra were acquired over extended periods of time from the same spot on the sample, spectral changes were detected attributable to radiation damage. The as-isolated form of the β subunit was more susceptible to radiation damage than Ti^{3+}-reduced samples. However, at the lowest temperature available, ~2 K, little or no change was observed in the as-isolated protein over time, even after 90 min of exposure to the X-ray beam. By contrast, at 20 K, with successive scans, a low energy shoulder emerged at about 852.0 eV and there was a decrease in the main peak intensity (see Supporting Information). This is presumably due to the formation of a Ni(I) species. Interestingly, both the rate and the spectral characteristics of the radiation damage changed between 100 and 20 K. At 100 K, with increasing dose, a new high-energy peak at 856.5 eV was found, which increased in intensity over the course of 2 h, while the main peak decreased (see the Supporting Information). The new spectrum was unlike any other model compound that we have yet studied and, given the decline in intensity in the main L_3 region, one possibility is that a Ni(0) species was produced.

The scan procedure in the L-edge chamber was optimized to minimize the influence of radiation damage. Because very little change was found after a short, 10 min exposure to the beam, even at 20 K, the L_3 and L_2 peak regions (which contain the chemically sensitive information and are most influenced by radiation damage) were scanned first, and the remaining three regions were scanned thereafter (below L_3, between L_3 and L_2, and above L_2). In the XMCD chamber, left and right-hand circularly polarized light were scanned consecutively on the same sample spot, and the total scan time at 2.2 K was 80 min.

A comparison of the quality of the Ni L-edge spectra obtained using the two chambers with the different detector systems was made using separate samples of the as-isolated ACDS β subunit (Figure 1). The

(13) Ralston, C. Y.; Wang, H.; Ragsdale, S. W.; Kumar, M.; Spangler, N. J.; Ludden, P. W.; Gu, W.; Jones, R. M.; Patil, D. S.; Cramer, S. P. *J. Am. Chem. Soc.* **2000**, *122*, 10553−10560.
(14) Friedrich, S.; Funk, T.; Drury, O.; Labov, S. E.; Cramer, S. P. *Rev. Sci. Inst.* **2002**, *73*, 1629−1631.
(15) Young, A. T.; Martynov, V.; Padmore, H. *J. Electron Spectrosc. Relat. Phenom.* **1999**, *103*, 885−889.
(16) Cramer, S. P.; Chen, J.; George, S. J.; van Elp, J.; Moore, J.; Tench, O.; Colaresi, J.; Yocum, M.; Mullins, O. C.; Chen, C. T. *Nucl. Inst. Methods A*, **1992**, *319*, 285−289.
(17) Funk, T.; Friedrich, S.; Young, A.; Arenholz, E.; Cramer, S. P. *Rev. Sci. Inst.* **2002**, *73*, 1649−1651.
(18) Cramer, S. P.; Peng, G.; Christiansen, J.; Chen, J.; van Elp, J.; George, S. J.; Young, A. T. *J. Electron Spectrosc. Relat. Phenom.* **1996**, *78*, 225−229.
(19) van der Laan, G.; Zaanen, J.; Sawatzky, G. A.; Karnatak, R.; Esteva, J.-M. *Phys. Rev. B*, **1986**, *33*, 4253−4263.

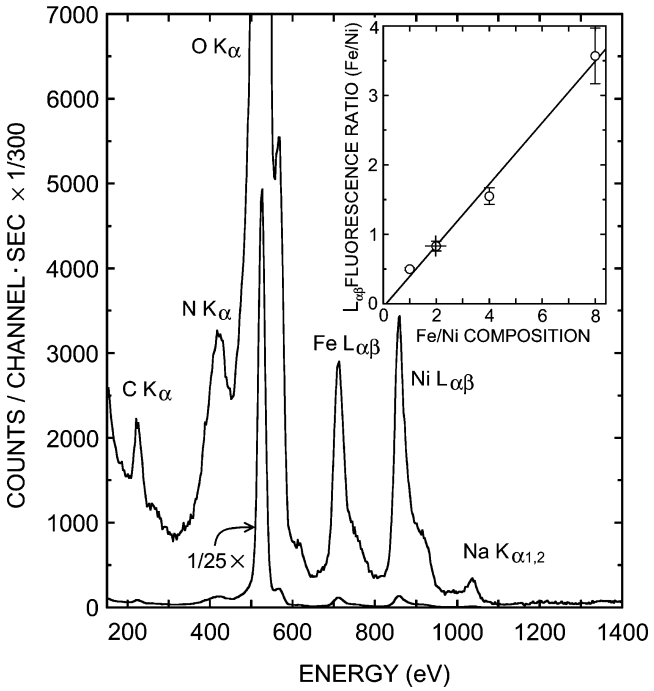

Figure 2. Soft X-ray emission spectrum of the 2:1 Fe:Ni standard used in the analysis of the ACDS β subunit. The STJ detector was used with excitation at 890 eV. No background subtraction was applied to the spectrum as shown, in which scattered radiation was minimized by positioning the detector at 90° relative to the beam in the plane of the synchrotron. The high-energy shoulders on all primary peaks arise from X-ray absorption in the lower detector layer.[14] The Na fluorescence is excited by second-order radiation. *Inset*, the measured Fe/Ni Lαβ fluorescence ratio plotted versus Fe/Ni composition of standards prepared as described under Experimental Procedures. The standards (○) were fit by linear least squares, solid line. The observed β subunit Fe/Ni fluorescence ratio is indicated by (+).

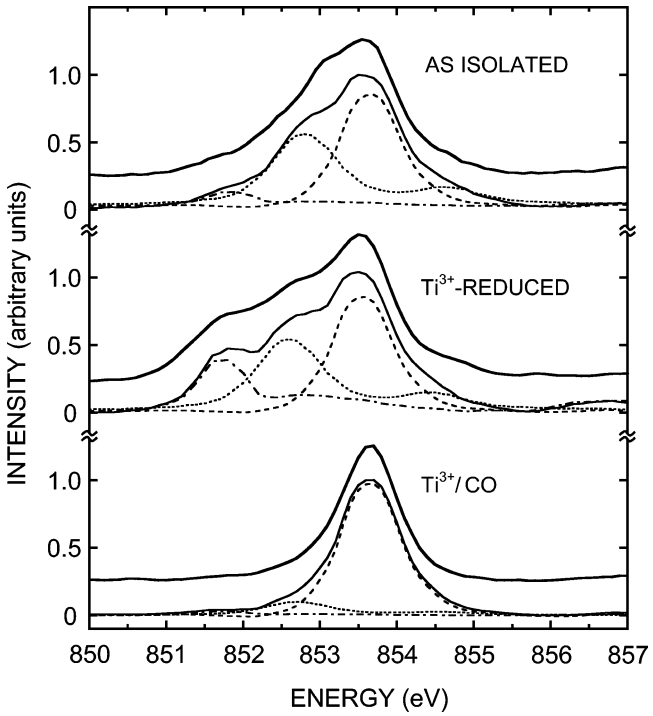

Figure 3. Ni L_3 edge spectra of the ACDS β subunit in the as-isolated, Ti^{3+}-reduced, and Ti^{3+}/CO forms, as indicated (−). Spectra of the components used for fitting are: $(Ph_4As)_2Ni(II)[S_2C_2(CF_3)_2]_2$ for low-spin Ni(II) (- - - -), $Ni(tren)_2$ for high-spin Ni(II) (••••) and [PhTt(tBu)]Ni-$(P(CH_3)_3)$[36] for Ni(I) (− • −). The spectrum of the Ni(I) model compound is shown shifted to higher energy by 0.1 eV in order to optimize the fit to the as-isolated form; the spectrum of the high-spin Ni(II) reference compound was shifted to lower energy by 0.3, 0.4 and 0.5 eV for fitting the as-isolated, Ti/CO, and Ti-reduced forms, respectively; and the low-spin Ni(II) dithiolene spectrum was shifted by 0.1 eV to higher energy for fitting the as-isolated and Ti/CO forms. Best fit combinations of the three components are indicated (−).

spectra displayed nearly identical signal-to-noise ratios, and were virtually superimposable. These data confirmed that both systems yield accurate, high quality spectra, and provide further evidence that radiation damage was negligible under the optimized conditions used in these studies.

Results and Discussion

Elemental Analysis. The Fe:Ni ratio in the ACDS β subunit was determined from the relative intensities of Fe and Ni Lαβ fluorescence signals. As shown in Figure 2, the STJ detector yielded emission spectra with well-resolved lines for O, Fe, and Ni. Because the absolute intensities are affected by geometrical factors, absorption cross sections, and fluorescence yields, a calibration curve was generated using standard samples with known Fe:Ni ratios. The Fe/Ni ratio for the β subunit thus obtained was 2.0 ± 0.3, Figure 2 inset. An Fe:Ni ratio of approximately 2:1 is consistent with the metal content analyses using Kα fluorescence[8] and plasma emission spectroscopy,[4] as expected for an enzyme with an A-cluster containing an $[Fe_4S_4]$ cluster and a binuclear Ni−Ni site.

Ni L-Edge Spectra. The Ni L_3 edges of the as-isolated, Ti^{3+}-reduced and Ti^{3+}/CO forms of the ACDS β subunit are shown in Figure 3. The peak in all three samples was found at ∼853.6 eV. However, the three spectra showed significant differences. The as-isolated and Ti^{3+}-reduced β subunit spectra had a broad L_3 edge (Figure 3, top and middle), whereas the CO/Ti^{3+}-treated β subunit had a much sharper L_3 edge (Figure 3, bottom). The spectrum of the as-isolated protein exhibited a strong, low energy component at ∼853.0 eV and a weak high energy shoulder at ∼ 854.4 eV, features that also are present in the Ti^{3+}-reduced form. Notably, an additional component of substantially lower energy was evident in the Ti^{3+}-reduced form at 851.7 eV (Figure 3, middle).

The $L_{2,3}$ spectrum of the Ti^{3+}/CO form of the β subunit was typical of spectra for complexes containing low-spin Ni(II). A comparison with one such compound, the low-spin Ni(II) complex $(Ph_4As)_2Ni(II)[S_2C_2(CF_3)_2]_2$ is shown in Figure 3, bottom. The L_3 centroid energy of 853.6 eV is consistent with values seen for low-spin Ni(II) systems.[13,20] Moreover, the branching ratio, $I(L_3)/I(L_2 + L_3)$, [21] was 0.63, which falls at the low end of the range 0.63−0.70 seen for low-spin Ni(II) model compounds (Table 1).[13,20,22] Thus, following Ti^{3+}/CO treatment nearly 100% low-spin Ni(II) could be assigned to both Ni sites in the β subunit A-cluster.

In comparison with the Ti^{3+}/CO spectrum, the as-isolated and Ti^{3+}-reduced $L_{2,3}$ spectra showed a trend toward higher branching ratios (0.73 and 0.76) and lower integrated intensities (17 and 13), respectively. As mentioned above, features were observed on both sides of the central 853.6 eV peak (at 853.0

(20) Wang, H.; Ralston, C. Y.; Patil, D. S.; Jones, R. M.; Gu, W.; Verhagen, M.; Adams, M. W. W.; Ge, P.; Riordan, C.; Marganian, C. A.; Mascharak, P.; Kovacs, J.; Miller, C. G.; Collins, T. J.; Brooker, S.; Croucher, P. D.; Wang, K.; Stiefel, E. I.; Cramer, S. P. *J. Am. Chem. Soc.* **2000**, *122*, 10544−10552.
(21) Thole, B. T.; van der Laan, G. *Phys. Rev. B*, **1988**, *38*, 3158−3171.
(22) Wang, H.; Patil, D. S.; Gu, W.; Jacquamet, L.; Friedrich, S.; Funk, T.; Cramer, S. P. *J. Electron Spectrosc. Relat. Phenom.* **2001**, *114*, 855−863.

Table 1. Ni L-edge Properties for the ACDS β Subunit Under Different Conditions

sample	$L_{2,3}$ intensity[a]	branching ratio[b]	L_3 centroid (eV)[c]
as-isolated	17.0(5)	0.730(9)	853.32(5)
Ti^{3+}-reduced	13.0(5)	0.756(9)	852.98(5)
Ti^{3+}/ CO	nd	0.632(9)	853.57(5)

[a] The $L_{2,3}$ intensity was calculated using the integrated L_3 and L_2 peaks with normalization to the continuum step. [b] The branching ratio is the ratio of integrated intensities $I(L_3)/I(L_2 + L_3)$. [c] The L_3 centroid energy was calculated using the first moment of the L_3 peak including all intensities within 80% of the maximum intensity.

and 854.4 eV), which are typical for spectra of high-spin Ni(II) species. The splitting of the high-spin Ni(II) L_3-edge can be explained as a multiplet feature due primarily to an exchange interaction between the partially occupied $2p^5$ and $3d^9$ shells in the final state.[23,24] For example, the L_3-edge of high-spin Ni(II)-azurin has a main peak at 852.7 eV with a high energy shoulder at 854.8 eV.[25] As indicated in Figure 3, top, most of the features in the as-isolated spectrum could be simulated using roughly equal fractions of $(Ph_4As)_2Ni(II)[S_2C_2(CF_3)_2]_2$ and Ni(II)$(tren)_2$ [tren = tris(2-aminoethyl)amine] as models for low-spin and high-spin Ni(II).

The branching ratios of 0.73 and 0.76 observed for the as-isolated β subunit and for the Ti^{3+}-reduced form are in the range of 0.71 to 0.77 expected for high-spin Ni(II) compounds from empirical studies. Theoretical considerations also hold that higher branching ratios signify a higher fraction of high-spin Ni(II) and/or Ni(I). Notably, the additional, prominent low-energy feature near 851.7 eV in the Ti^{3+}-reduced spectrum is present in a region indicating Ni(I).

Other parameters of the L-edge spectrum provided further support for the existence of Ni(I) in the Ti^{3+}-reduced form. One of these was the increased branching ratio found relative to the as-isolated enzyme, because Ni(I) complexes are known to have the highest values of branching ratio. Another was the decrease in integrated intensity observed from 17 in the as-isolated enzyme to 13 in the Ti^{3+}-reduced form. This indicates formation of a substantial quantity of Ni(I), due to the lower transition probability of the d^9 system, in which a value of 8.7 has been ascribed to one hole.[26] In simulations using three components (Figure 3, middle) the Ti^{3+}-reduced spectrum could be fit by assigning 25−30% Ni(I), similar amounts of high-spin Ni(II) and about 40% low-spin Ni(II). Approximately equal quantities of Ni(I) were observed in samples treated with 1 mM and 4 mM Ti^{3+}-citrate.

Surprisingly, during the course of these investigations, we observed that the spectrum of the Ti^{3+}/CO sample was not stable, and was altered upon removal of CO during the time required for mounting of the disks and transfer to the vacuum chamber − demanding that this step be completed rapidly. Otherwise, the spectrum observed for Ti^{3+}/CO samples tended to revert over time toward the spectrum of the as-isolated sample, as shown in Figure 4. The spectrum of samples for which this time was minimized (about 10 min) showed only the low-spin Ni(II) species. However, extending the time to 50 min resulted in the formation of a low-energy and a high-energy shoulder in the spectrum. These features were close to the ones in the spectrum of the as-isolated sample. Thus, a fraction of the low-spin Ni(II) was converted to a high-spin Ni(II) species, which appeared to correlate with loss of CO from the sample.

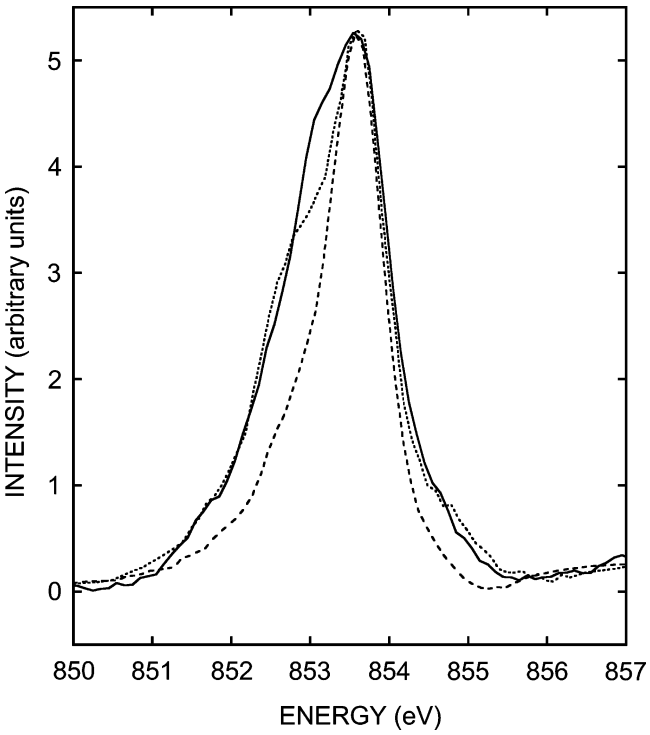

Figure 4. Tendency of the Ti^{3+}/CO form to revert to a spectrum resembling the as-isolated enzyme following removal from a CO atmosphere. Samples dried under 100% CO, as described under Experimental Procedures, were transferred to the capped sample holder under N_2, and held for either 10 min (- - - -) or 50 min (••••) before loading into the chamber, cooling to 77 K and uncapping. The spectrum of the as-isolated protein is shown for comparison (−).

Ni XMCD Spectra. Soft X-ray MCD is a relatively new tool for characterization of metal centers in proteins.[27,28] This probe has the advantage of selectivity for paramagnetic centers and sum rules that provide information about spin and orbital magnetic moments.[27,28] Ni L-edge XMCD spectra for the ACDS β subunit under different conditions are shown in Figure 5. The as-isolated enzyme (Figure 5A) exhibited an XMCD effect of about −18% at the XMCD minimum of 852.8 eV, in the region where the absorption spectrum exhibits the low energy component, and displayed a positive XMCD signal near at 854.7 eV, where the high-energy absorption shoulder occurs. This bipolar L_3 signal is typical for high-spin Ni(II) species.[29,30] The XMCD in the L_2 region is unipolar and positive. No XMCD effect was observed for the main peak at 853.6 eV.

The strongest XMCD effect was observed for the Ti^{3+}-reduced form of the β subunit (Figure 5B), with a value of nearly

(23) van der Laan, G.; Thole, B. T.; Sawatzky, G. A.; Verdaguer, M. *Phys. Rev. B*, **1988**, *37*, 6587−6589.
(24) Wang, X.; Grush, M. M.; Froeschner, A. G.; Cramer, S. P. *J. Synchrotron Rad.* **1997**, *4*, 236−242.
(25) Funk, T.; Kennepohl, P.; Wehbi, W. A.; Di Bilio, A. J. Young, A. T.; Friedrich, S.; Arenholz, E.; Gray, H. B.; Cramer, S. P. *X-ray Magnetic Circular Dichroism of Pseudomonas aeruginosa Nickel(II) Azurin*; **2003**, manuscript submitted to *J. Am. Chem. Soc.*.
(26) Wang, H.; Ge, P.; Riordan, C. G.; Brooker, S.; Woomer, C. G.; Collins, T.; Melendres, C. A.; Graudejus, O.; Bartlett, N.; Cramer, S. P. *J. Phys. Chem. B*, **1998**, *102*, 8343−8346.
(27) Cramer, S. P.; Wang, H.; Bryant, C.; Legros, M.; Horne, C.; Patel, D.; Ralston, C.; Wang, X. In *Spectroscopic Methods in Bioinorganic Chemistry*; Solomon, E. I. and Hodgson, K. O., Ed.; American Chemical Society: Washington, D. C., 1998; Vol. 692, pp 154−178.
(28) Cramer, S. P., in Telser, J., Ed.; ACS, 2003, pp. in press.
(29) de Groot, F. M. F.; Arrio, M.-A.; Sainctavit, P.; Cartier, C.; Chen, C. T. *Phys. B*, **1995**, *208−209*, 84−86.
(30) van der Laan, G.; Thole, B. T. *Phys. Rev. B*, **1991**, *43*, 13401−13411.

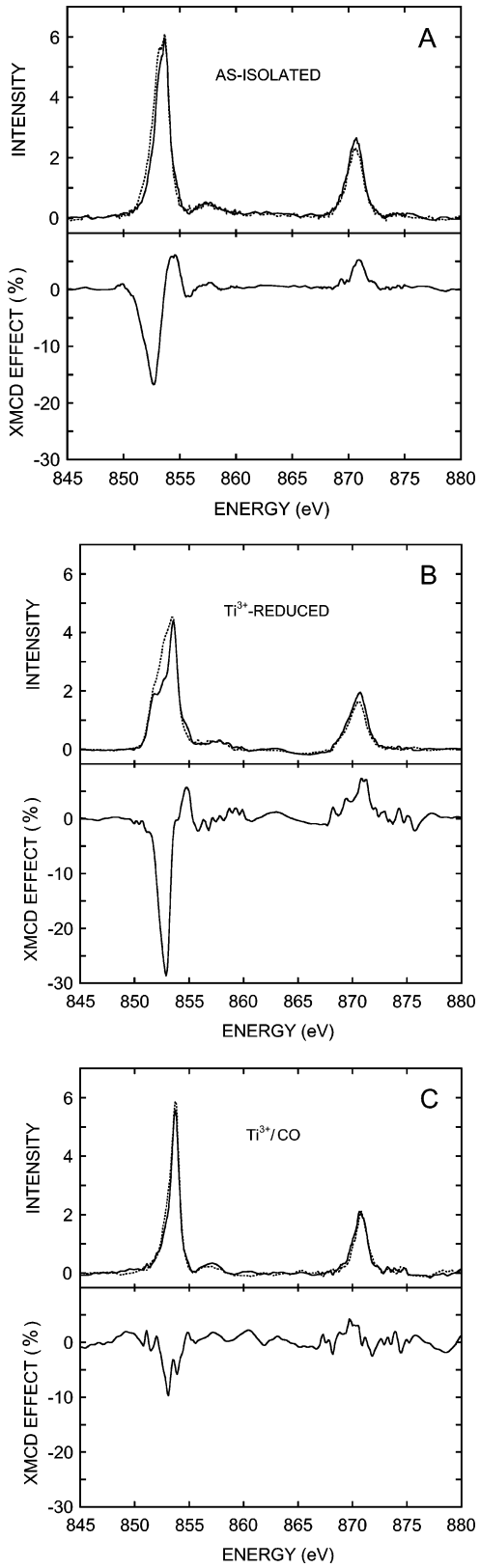

Figure 5. Ni $L_{2,3}$-edge XMCD spectra of different forms of the ACDS β subunit. L-edge absorption spectra were recorded with right (−) and left (- - -) circularly polarized light, upper. The edge jumps have been removed by separate background subtractions using a two-step function, with a secondary background component subtracted using a parabolic function. XMCD spectra, lower, were calculated as the difference in intensity, right-minus-left, normalized to the L_3 peak maximum (XMCD effect, %). The spectra were taken at 6 T and 2.2 K. Samples were as indicated: **A**, as-isolated; **B**, Ti^{3+}-reduced, and **C**, Ti^{3+}/CO treated.

−30% at the XMCD minimum at 852.8 eV.[31] The general shape of the XMCD spectrum was similar to that of the as-isolated state, confirming its high-spin Ni(II) character. In addition, T−T multiplet simulations[32] provided a reasonable fit to the observed XMCD spectrum using a high-spin Ni(II) center in a tetrahedral ligand field (see the Supporting Information). Minor differences in the spectra of the Ti^{3+} and as-isolated forms, that are close to the presently existing signal-to-noise limitations, may indicate that the signal comes from slightly different high-spin Ni(II) species, perhaps as a result of changes taking place in a nearby group such as reduction of the $[Fe_4S_4]$ cluster.

The Ni XMCD spectrum for the Ti^{3+}/CO form showed a very small XMCD effect (Figure 5C), as expected from the assignment of low-spin Ni(II) described above. Such small magnitude effects might have resulted from an imperfect subtraction and normalization procedure for left circularly polarized and right circularly polarized spectra. However, given the apparent instability of the Ti^{3+}/CO form (as discussed above), the residual XMCD effect also might be due to traces of a regenerated high-spin form. In either case, the effect is small, and not reflective of the predominantly low-spin Ni(II) character of the Ti^{3+}/CO form, as evident from the XMCD results.

Conclusion

The A-cluster in the methanogen ACDS β subunit active site shares a number of spectroscopic and enzymological properties with the bacterial CODH/ACS A-cluster, which, taken together with recent results from site directed mutagenesis analyses, indicate an arrangement of metals with similar geometries and coordination environments. Metal analyses by plasma emission spectroscopy,[4] Ni and Fe Kα fluorescence intensity ratios,[8] and the results presented here from quantitative Ni and Fe L-edge fluorescence ratios all indicate 2 Ni atoms per $[Fe_4S_4]$ cluster with no significant levels of other metals including Cu and Zn.

Several different A-cluster structures have been presented from previous crystallographic studies on CODH/ACS which vary in their metal compositions and in the geometry of the metal site proximal to the $[Fe_4S_4]$ cluster. The results from Ni K-edge XANES and EXAFS analyses on the ACDS β subunit here are interpreted in terms of a model of the A-cluster in the methanogen enzyme generally similar to those found in the bacterial CODH/ACS, but with Ni present at both sites in the Ni−Ni binuclear center bridged to the $[Fe_4S_4]$ cluster.[8] From these studies, in connection with crystallographic results on CODH/ACS,[6,7] different geometries were proposed for the individual Ni sites in the β subunit A-cluster, corresponding to square planar for the Ni site distal to the $[Fe_4S_4]$ cluster, designated Ni_b, and tetrahedral or distorted tetrahedral for the proximal site, Ni_a (see Scheme 1 in ref 8). The results from the present study provide additional evidence for these assignments,

(31) The reason for the increase in XMCD effect, from −18% in the as-isolated enzyme to −29% upon reduction with Ti^{3+} remains uncertain. In this regard, it may be notable that exposure of Ti^{3+}-reduced samples to air, which causes a complete loss of the Ni(I) signal in the L-edge spectrum, also resulted in increased intensity in the region near 853.0 eV, as well as in the high energy shoulder region around 854.4 eV, apparently due to generation of a more ionic high-spin Ni(II) form. However, air oxidation is an unlikely explanation for these samples, which display substantial quantities of Ni-(I). Since the high-spin Ni(II) component in these samples exhibited slightly shifted centroids and slightly different splitting, a change in magnetic behavior might have resulted as well.

(32) The T−T Multiplets suite of programs was graciously provided by Dr. Frank de Groot, and is available at http://www.anorg.chem.uu.nl/de-groot.htm.

and show further that the two Ni sites differ significantly in their individual chemical properties.

The A-cluster in the as-isolated ACDS β subunit contained predominantly two types of Ni in roughly equal amounts, corresponding to high-spin Ni(II) and low spin Ni(II), as indicated by the results from L-edge measurements (Figure 3, top), and supported by XMCD analyses (Figure 5A). From basic ligand field theory, a square planar site for Ni(II) invariably produces a low-spin configuration, whereas a tetrahedral site favors a high-spin configuration. Thus, it is proposed that the high-spin species corresponds to tetrahedral or distorted tetrahedral Ni(II) located at the proximal site (where the distortion from tetrahedral cannot rule out 5-coordinate geometries), and that the low-spin fraction in the as-isolated form represents the signal from Ni(II) in square planar geometry at the distal site. As shown in Figure 3, top, ~10% of Ni(I) was used in the fit of the as-isolated form. Although this may suggest some amount of Ni(I) present in the enzyme as isolated, another possibility is that it represents a small degree of X-ray photoreduction.

The appearance of an ~30% Ni(I) fraction in the Ti^{3+}-reduced samples is most naturally ascribed to reduction of the tetrahedral Ni(II) species. In parallel, a substantial decline in the high-spin Ni(II) fraction was evident (see Figure 3), but there also was a decrease in low-spin Ni(II). One possibility is that both the proximal and distal Ni sites are capable of becoming reduced, however, reduction of Ni(II) in a square planar configuration is unexpected. An alternate explanation could involve two forms of the A-cluster in equilibrium with one another, in which the proximal Ni site is either tetrahedral, in high-spin configuration, or distorted square planar, in a low-spin state. In this situation, a decrease in the amount of the tetrahedral form upon reduction to Ni(I) also would cause decline in the amount of the low-spin form. Potentially, these two forms could reflect an equilibrium between different conformational states of the enzyme. In either case, the present work provides the first direct demonstration of Ni(I) formation in the A-cluster, and in addition indicates that the Ni(I) is generated at the proximal site.

The finding that the level of Ni(I) was not increased by increasing the Ti^{3+} concentration from 1 mM to 4 mM is further evidence for reduction of only one class of Ni sites. These results support a mechanism involving Ni(I) as a nucleophilic species formed in 1-electron reductive activation of the enzyme, potentially involved in attack on acetyl-CoA to form an activated enzyme-acetyl intermediate. Formation of Ni(0) was not observed, except in experiments for assessing radiation damage at high-temperature and long-term X-ray exposure. Since our analyses did not require Ni(0), little or no evidence could be obtained for a mechanism involving Ni(0).

One of the more remarkable findings was the nearly quantitative conversion of the high-spin Ni(II), at the proximal site Ni, to low-spin Ni(II) in the Ti^{3+}/CO treated form. Previously, it was postulated that CoA and CO bind to the proximal metal,[6] and recently direct evidence for CoA interaction in the coordination sphere of Cu^{1+} at the proximal site was obtained by EXAFS analysis of CODH/ACS with seleno-CoA bound as a substrate analogue.[33] The results of L-edge and XMCD analyses now provide the first direct evidence for reaction of CO at the proximal site Ni in the ACDS β subunit, converting the high-spin Ni(II) fraction nearly completely to a low-spin state.

A scenario in which CO reacts with Ni(I) to form a Ni(I)−CO adduct, followed by transfer of an electron to the $[Fe_4S_4]^{2+}$ cluster resulting in $[Fe_4S_4]^{1+}$ and Ni(II)−CO appears unlikely. In this regard, the formation of an $[Fe_4S_4]^{1+}$ form in the A-center NiFe−CO adduct was all but excluded on the basis of equivalent values of the isomer shift found in Mössbauer experiments in the oxidized versus CO-treated CODH/ACS α subunit.[34] In addition, our results from Fe EXAFS and XANES indicated less disorder in the ACDS β subunit $[Fe_4S_4]$ cluster and less reduction of the cluster by Ti^{3+} when the reaction was carried out in the presence of CO.[8]

One possibility for spin state conversion in the Ti^{3+}/CO form would be a reaction with CO resulting in direct transition at the high-spin Ni(II) site to generate a low-spin Ni(II)−CO form (along with the exchange of one electron with some other group in the process of $S = 1$ to $S = 1/2$ conversion). This is supported by the finding that direct addition of CO to the enzyme containing only Ni(II), and no other source of reducing agent, was capable of generating high levels of the NiFe−CO EPR signal.[4] Our finding of largely diamagnetic Ni(II) in the Ti^{3+}/CO form suggests that the A-center radical is located primarily at a site other than Ni, since spin states corresponding to either Ni(I) or Ni(III) were conspicuously absent in this form.

After CO is bound, formation of Ni(I) appears to be more difficult, since Ni(I) was not observed in the Ti^{3+}/CO reacted samples even at concentrations of Ti^{3+} citrate that otherwise would cause substantial reduction in the absence of CO. This would agree with a mechanism proposed earlier in which reduction of the enzyme-CO adduct to a form involved in the catalytic cycle was considered to be unlikely, particularly in the absence of other substrates.[4] In addition, the inability to reduce the enzyme in the presence of CO argues for an ordered mechanism in which CO binding would take place after methylation—also consistent with the inhibitory effects of high concentrations of CO noted for CODH/ACS by others.[35]

One interesting and still puzzling finding was the difference between samples treated with Ti^{3+}/CO and those reacted with CO alone. As noted in the accompanying study, samples treated with CO in the absence of Ti^{3+} citrate exhibited Ni and Fe K-edge spectra differing little from those of the as-isolated enzyme.[8] L-edge spectra also were taken on samples treated with CO alone (not shown) and exhibited similar behavior, i.e., little or no change from that of the β subunit as-isolated. Thus, the L-edge and K-edge data were fully consistent with one another, however, such behavior does not agree with the previous demonstration that the formation of the NiFe−CO EPR signal is independent of Ti^{3+} citrate.[4] One possibility is that Ti^{3+} citrate may act as a stabilizer for the Ni(II)-CO radical species, and therefore would be required in X-ray absorption studies, whereas it is unnecessary for EPR measurements under milder conditions. Direct irradiation of EPR samples could serve as one method for further study of these differences.

(33) Seravalli, J.; Gu, W.; Tam, A.; Strauss, E.; Begley, T. P.; Cramer, S. P.; Ragsdale, S. W. *Proc. Nat. Acad. Sci.* **2003**, *100*, 3689−3694.
(34) Xia, J. Q.; Hu, Z. G.; Popescu, C. V.; Lindahl, P. A.; Münck, E. *J. Am. Chem. Soc.* **1997**, *119*, 8301−8312.
(35) Maynard, E. L.; Sewell, C.; Lindahl, P. A. *J. Am. Chem. Soc.* **2001**, *123*, 4697−4703.
(36) Schebler, P. J.; Mandimutsira, B. S.; Riordan, C. G.; Liable-Sands, L. M.; Incarvito, C. D.; Rheingold, A. L. *J. Am Chem. Soc.* **2001**, *123*, 331−332.

In summary, Ni L-edge spectra of the ACDS β subunit A-cluster have been interpreted as evidence for a low-spin Ni-(II) at the distal Ni site, and a proximal site that can exist in a variety of forms: low-spin and high-spin Ni(II), Ni(I), and low-spin Ni(II)−CO. The paramagnetism of the high-spin Ni(II) species has been confirmed by XMCD spectroscopy. The higher resolution of soft X-ray spectroscopy complements interpretations involving two distinct Ni sites. Additional experiments with A-cluster derivatives that contain a single type of Ni are in progress.

Acknowledgment. The authors thank Drs. E. I. Stiefel and K. Wang for the sample of $(Ph_4As)_2Ni(II)-[S_2C_2(CF_3)_2]_2$. We thank Drs. T. Young and E. Arenholz for their assistance with the EPU beamline. This work was supported by the National Institutes of Health Grants GM-44380 and GM-65440 (S.P.C.), the National Science Foundation Grant MCB-0215160 (D.A.G.), the U.S. Department of Energy Grant DE-FG02-00ER15108 (D.A.G), and the U.S. Department of Energy, Office of Biological and Environmental Research. The ALS is supported by the U.S. Department of Energy, Office of Basic Energy Sciences.

Supporting Information Available: L-edge spectra from control experiments showing the effects of radiation damage as a function of X-ray beam exposure time and temperature (Figure S1), and a simulation of the XMCD spectrum of the Ti^{3+}-reduced β subunit using the T−T multiplet package assuming a high-spin Ni(II) species in tetrahedral geometry (Figure S2). This material is available free of charge via the Internet at http://pubs.acs.org.

JA0366033